PAPER

Check for updates

Hierarchical non-woven fabric NiO/TiO$_2$ film as an efficient anode material for lithium-ion batteries†

Hong Zhang,[a] Binqiang Tian,[a] Jian Xue,[a] Guoqing Ding,[b] Xiaoming Ji (ID) *[a] and Yang Cao (ID) *[b]

Hierarchical non-woven fabric NiO/TiO$_2$ film is prepared using a facile two-step synthesis by electrospinning and subsequent hydrothermal reaction to yield TiO$_2$ film decorated with NiO nanosheets. As an anode material for Li-ion batteries, the NiO/TiO$_2$ composite exhibits discharge and charge capacities of 1251.3 and 1284.3 mA h g^{-1}, with good cycling performance and rate capability. Characterization shows that the NiO nanosheets are distributed on the surface of the TiO$_2$ nanofibers. The total specific capacity of NiO/TiO$_2$ is higher than the sum of pure TiO$_2$ and NiO, indicating a positive synergistic effect of TiO$_2$ and NiO on the improvement of electrochemical performance. The results suggest that non-woven fabric NiO/TiO$_2$ film is a promising anode material for lithium ion batteries.

1. Introduction

With the rapid development of human society, the demand for green energy is increasing dramatically.[1,2] Owing to the high voltage, high capacity, and long cycle life, rechargeable lithium-ion batteries (LIBs) have become power sources for portable electronic devices and electric vehicles.[3] Graphite, a commercial anode material for LIBs, exhibits a low theoretical capacity (372 mA h g^{-1}) and poor rate capability, and thus cannot meet the increasing requirements of high-performance electrode materials.[4,5] Comparatively, transition metal oxides (TMOs), due to their high theoretical capacities and superior electrochemical properties, have attracted much attention as alternative anode materials. In particular, nickel oxide (NiO) is regarded as one of the most appealing anode materials because of its high theoretical capacity (718 mA h g^{-1}), high density (6.67 g cm^{-3}), low cost, environmental benignity, and natural abundance.[6,7]

Unfortunately, the poor electrical and ionic conductivities of NiO hinder its electrochemical performances.[8–10] Besides, the sluggish kinetics of the conversion reaction and the large volume expansion (95.69%) of the large-sized electrode materials severely restrict the development of NiO anodes.[11] To address these shortcomings, Poizot *et al.* first proposed the nano-sized TMOs that undergo conversion reactions with lithium and provide two- or three-fold higher reversible capacity than graphitic anodes.[12] After that, great efforts have been made

to improving the performance of NiO as the anode material through fabricating various nanostructures, including nanoparticles,[13] nanosheets,[14] nanotubes,[15,16] nanofibers,[17] hollow microspheres,[18,19] and sandwich-like films.[20] The nanoscaled materials not only shorten the electron and Li$^+$ diffusion pathways, but also increase the electrode–electrolyte interface, enhancing the cycling stability and high-rate capacity.[21,22] Nevertheless, the issues for nanoscaled materials are that they can easily become aggregated and get more structural defects, resulting in poor cycling performance.[23] Thus, sophisticated nanomaterials, particularly with designed unique structures, are highly needed.

Herein, a novel hierarchical non-woven fabric film composed of NiO nanosheets (NSs) grown on TiO$_2$ nanofibers is prepared *via* an electrospinning method combined with a hydrothermal post-treatment and used as an efficient anode material for LIBs. The special three-dimensional (3D) nanoarchitecture possesses outstanding advantages. First, the direct growth of NiO nanosheets on TiO$_2$ nanofibers improves the conductivity and separates active materials from each other, completely avoiding the aggregation and agglomeration. In addition, this 3D morphology helps to shorten the pathways for Li$^+$ and electron transport and enlarges exposed surface for more lithium-exchange channels, leading to high rate capability and cycling stability.

2. Experimental

2.1 Material fabrication

All chemicals or materials were used directly without further purification. First, the non-woven fabric film composed of TiO$_2$ nanofibers is prepared according to our previous report.[24,25] Then, the as-prepared TiO$_2$ non-woven fabric film was employed

[a]College of Tobacco Science, Henan Agricultural University, Zhengzhou, Henan, 450002, China. E-mail: xiaomingji@henau.edu.cn

[b]College of Material and Chemical Engineering, Zhengzhou University of Light Industry, Zhengzhou, Henan 450002, China. E-mail: 2016055@zzuli.edu.cn

† Electronic supplementary information (ESI) available. See DOI: 10.1039/c9ra04947a

as the scaffold for the growth of NiO nanosheets *via* a hydrothermal reaction. Briefly, the non-woven fabric film was tilted against the wall of the autoclave at a certain angle. 5 mmol of $NiSO_4 \cdot 6H_2O$ and 10 mmol of hexamethylenetetramine (HMT) were added to 60 mL of water to form a homogeneous green solution. Subsequently, the solution was transferred into the autoclave, which was then tightly sealed and kept in an electric oven at 100 °C for 12 h. After cooling down naturally to room temperature, the non-woven fabric film was then taken out, washed with water thoroughly, and dried at 60 °C overnight. The obtained non-woven fabric film was placed in a tube furnace and annealed in air at the temperature of 450 °C with a heating rate of 2 °C min^{-1}. After cooling to room temperature, the resultant non-woven fabric film was donated as NiO/TiO$_2$ film.

2.2 Structure characterization

The compositions of the as-prepared materials were examined by X-ray diffraction (XRD, D8-ADVANCE) with Cu Kα radiation. The morphology and elemental distributions of the samples were investigated by a field emission scanning electron microscope (FE-SEM, JSM-7001F) equipped with energy dispersive X-ray spectroscopy (EDS) and a transmission electron microscope (TEM, JEM-2100).

2.3 Electrochemical measurements

Electrochemical measurements were carried out in CR2016 coin-type cells. The testing cells were assembled in an argon-filled glove box using NiO/TiO$_2$ non-woven fabric film and Li foil as the working electrode and counter electrode, respectively. Celgard 2400 as the separator, and 1 mol L^{-1} LiPF$_6$ in a 1 : 1 (volume) mixture of ethylene carbonate and ethyl methyl carbonate as the electrolyte. The charge/discharge test was performed between 0.01 V and 3 V at various current densities using a NEWER battery tester. Cyclic voltammetry (CV, 0.01 V to 3 V, 0.1 mV s^{-1}) and electrochemical impedance spectroscopy (EIS, 0.01 to 10^5 Hz) were conducted using electrochemical workstation (CHI 660E) with 5 mV amplitude. All tests were carried out at room temperature.

3. Results and discussion

The 1D nanostructures with fewer surface defects are well recognized as efficient for fast electron transport.[26] To preserve the long fibrous structure of the electrospinning nanofiber, TiO$_2$ non-woven fabric film was used as the current collector, and NiO NSs are grown on the surface of nanofibers after the hydrothermal treatment. The detailed fabrication procedure is illustrated in Scheme 1. Briefly, an electrospinning process was used to synthesize TiO$_2$ non-woven fabric film, which was then employed as the scaffold for the growth of NiO nanosheets *via* a hydrothermal reaction. The composite material film was obtained by calcining in air at 450 °C for 2 h to decompose Ni(OH)$_2$ to NiO.

The XRD patterns of the samples are shown in Fig. 1. The TiO$_2$ film exhibits diffraction peaks that agree well with the characteristic peaks of anatase TiO$_2$ crystal. Namely, the peaks at 25.4, 48.1 and 54.6° correspond to the (101), (200) and (105) crystal planes of TiO$_2$ (JCPDS card no. 21-1272), respectively. All the reflections of NiO sample can be perfectly indexed as NiO (JCPDS card no. 65-2901) in terms of the relative intensity and position. The well-resolved diffraction peaks appearing at 37.08, 43.23, and 62.81° are correspondingly assigned to the (111), (200), and (220) planes, respectively. For the NiO/TiO$_2$ film, all the diffraction peaks are in agreement with the standard patterns of TiO$_2$ (JCPDS card no. 21-1272) and NiO (JCPDS card no. 65-2901), and no impurity diffraction peaks are observed.

The morphologies of the samples were examined by field-emission scanning electron microscope (SEM) and transmission electron microscope (TEM). Fig. 2 shows the SEM images of the TiO$_2$ nanofibers (Fig. 2a and b) and the NiO/TiO$_2$ composite (Fig. 2c and d). It can be seen that the electrospinning TiO$_2$ nanofibers have a relatively smooth surface with diameters ranging from 350 to 700 nm, which are intact during the film fabrication process. The long fiber structure should be effective in facilitating electron transport. The nanofibers stack loosely with each other, leaving lots of voids, which facilitate the electrolyte penetration as well as Li$^+$ transport between the electrode and the electrolyte. After the hydrothermal treatment, as shown in Fig. 2c and d, each nanofiber is coated with NiO nanosheets with the average thickness of ∼7 nm and height of ∼350 nm. The TEM analyses (Fig. 2e and f) also demonstrate the highly branched structure, in which NSs are disorderly grown on the surface. The high-resolution TEM (HR-TEM) image (Fig. 2g) of a single NS shows a typical lattice distance of 0.21 nm, which is indexed to the (200) plane of NiO. Compared with the pristine TiO$_2$ nanofiber film, the large interspaces between fibers are filled with NSs, resulting in more active sites of the composite film. The corresponding element mapping of Ti, O, and Ni in Fig. 3 also confirms the uniform dispersion of NiO nanosheets on the TiO$_2$ fiber surface. However, in the absence of TiO$_2$ nanofibers, NiO NSs tend to self-assemble into nanoflowers with sizes ranging from 6 to 10 μm (Fig. S1†).

Cyclic voltammetry (CV) tests and galvanostatic discharge/charge measurements were investigated in half-cell configurations to evaluate the lithium storage properties of the as-prepared NiO/TiO$_2$ composite film as an anode electrode in LIBs. Fig. 4a shows the CV curves of the NiO/TiO$_2$ film for the 1st and 2nd cycles at a scan rate of 0.01 mV s^{-1} over the voltage range of 0.01–3 V. In the first cathodic scan, a strong peak appears at ∼0.47 V, which corresponds to the formation of a solid electrolyte interphase (SEI) film and the reduction of NiO to Ni.[27] In the following cycle, this cathodic peak significantly shifts to about 0.9 V, which agrees well with previous reports.[28,29] The anodic scans show similar profiles, in which two oxidation peaks are found at 1.49 V and 2.1 V, indicating the decomposition of the SEI film and the oxidation of Ni to NiO, respectively.[30]

Fig. 4b and c show the discharge/charge curves of NiO and NiO/TiO$_2$ electrodes at 0.1C and 0.2C (1C = 718 mA h g^{-1}), respectively. The NiO electrode exhibits discharge and charge capacities of 615.8 and 662.6 mA h g^{-1} at 0.1C, and 626.4 and 579.6 mA h g^{-1} at 0.2C. Impressively, the NiO/TiO$_2$ electrode
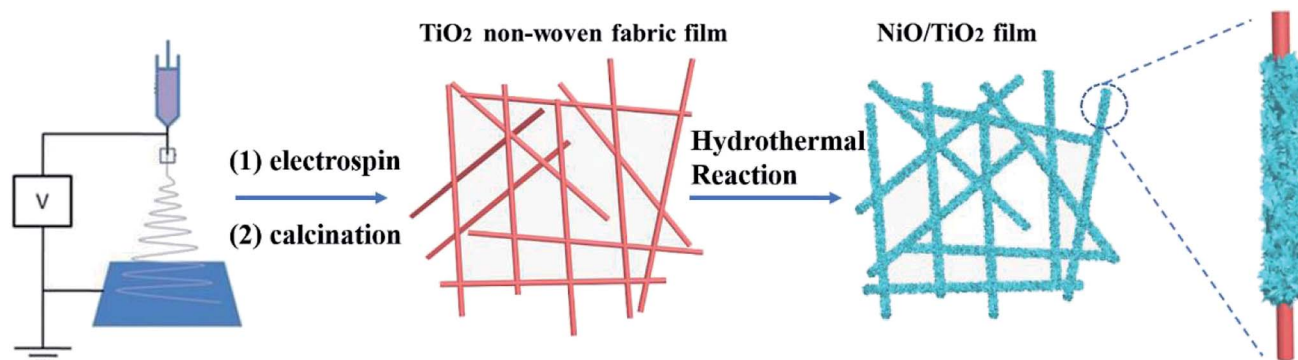
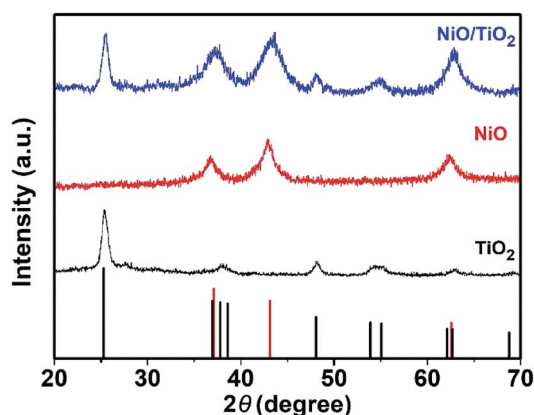**Scheme 1** Schematic diagram for the fabrication of the hierarchical NiO/TiO$_2$ film.

Fig. 1 XRD patterns of the TiO$_2$, NiO and NiO/TiO$_2$, respectively.

exhibits discharge and charge capacities of 1251.3 and 1284.3 mA h g^{-1} at 0.1C, and 1075 and 1154.4 mA h g^{-1} at 0.2C, with the coulombic efficiency of 97% and 93%, respectively. Thus, the discharge and charge capacities of the NiO/TiO$_2$ electrode are about twofold of those delivered by the NiO electrode.

The electrochemical performance is crucial for the potential anode materials in LIBs. The rate performance of the NiO/TiO$_2$ electrode is first examined at different charge/discharge rates from 0.05C to 0.5C for 5 cycles, and then returns to 0.05C. As illustrated in Fig. 4d, the NiO/TiO$_2$ electrode exhibits high discharge capacities at lower current densities, which is 1388.9 mA h g^{-1} at the rate of 0.05C and decreases to 509.5 mA h g^{-1} at 0.5C. When the current returns to 0.05C, the discharge capacity recovers to 1015 mA h g^{-1}, showing good
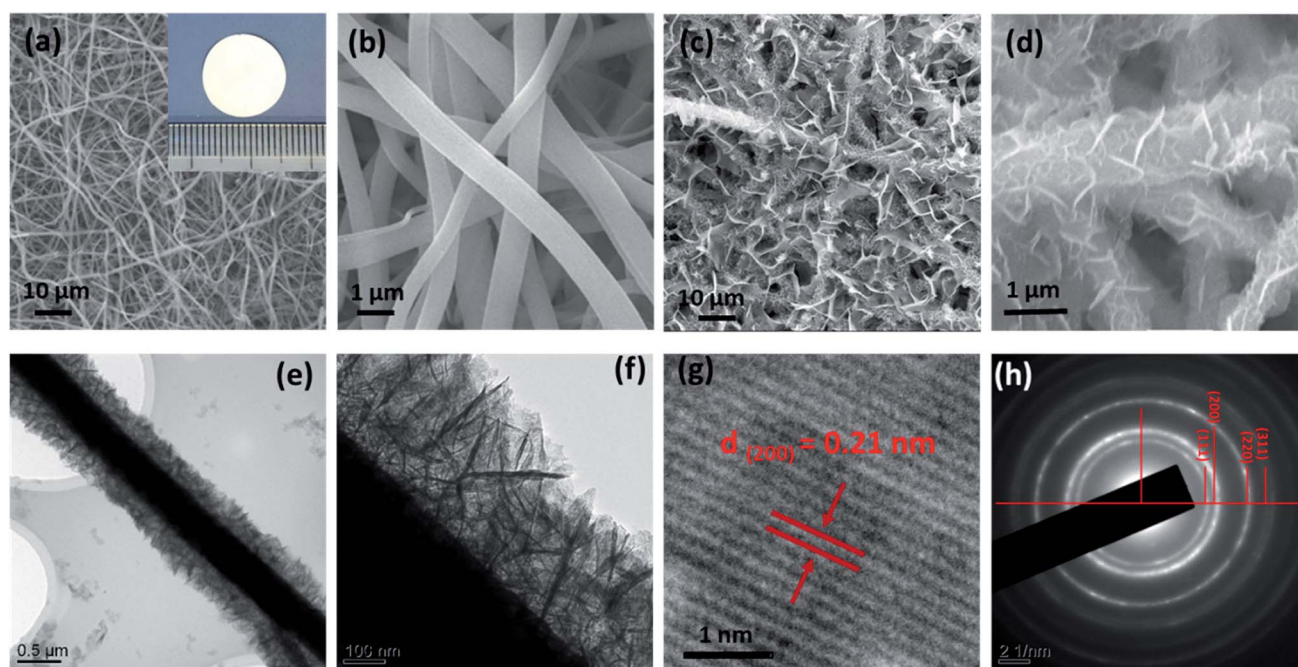

Fig. 2 (a) Low- and (b) high-magnification SEM images of the TiO$_2$ fibers. The inset figure shows the TiO$_2$ electrode. (c) Low- and (d) high-magnification SEM images of the NiO/TiO$_2$ composite film. (e and f) TEM images of the NiO/TiO$_2$ composite. (g) HRTEM and (h) SAED images of NiO NS.
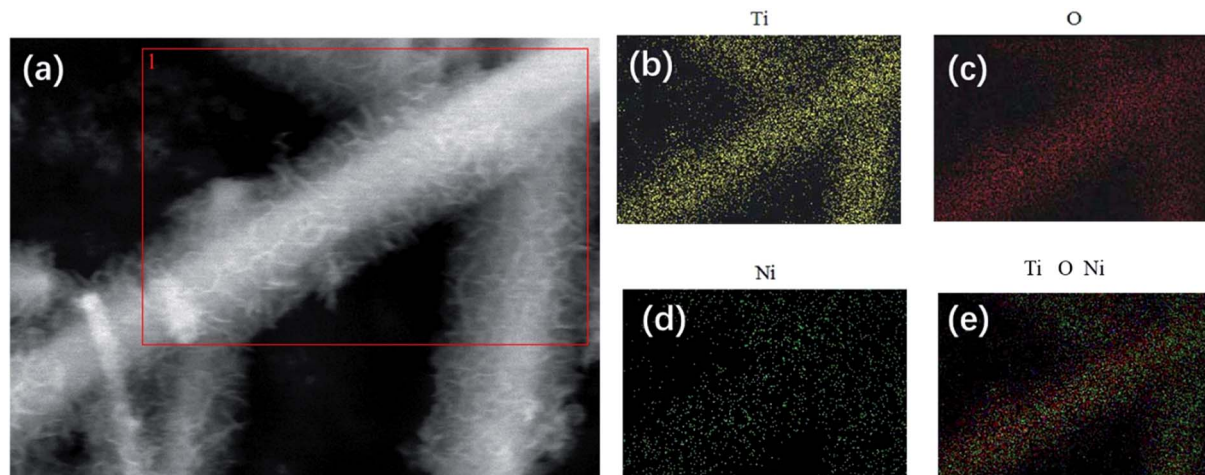
Fig. 3 (a) SEM image of NiO/TiO$_2$ and (b−e) the corresponding EDX element mapping of (b) Ti, (c) O, (d) Ni, and (e) the reconstructed chemical map.

stability. Fig. 4e presents the cycling performance of the two electrodes. The initial discharge capacity of NiO/TiO$_2$ electrode is 1285.6 mA h g^{-1}, and the capacity maintains a high value of 487.1 mA h g^{-1} after 50 cycles at 0.1C. While for the NiO electrode, the initial discharge capacity is 655.2 mA h g^{-1}, decreasing to only 198.9 mA h g^{-1} after 50 cycles.

To confirm the electrochemical kinetics related to Li$^+$ diffusion, electrochemical impedance spectroscopy (EIS) measurements were carried out. Fig. 4f presents the Nyquist plots of the electrodes in the frequency range of 10^{-2} to 10^5 Hz at the open-circuit potential. The semicircle in the high-frequency region is

attributed to the charge transfer resistance (R_{ct}) at the electrode–electrolyte interface, and the inclined line in the low-frequency range (the Warburg impedance) corresponds to Li-ion diffusion in the electrode.[31] The NiO/TiO$_2$ electrode shows the lowest R_{ct} and Warburg impedance among the testing electrodes. The low R_{ct} is ascribed to the high number of electroactive sites due to the good dispersion of NiO nanosheets, while the tunneled TiO$_2$ nanofibers shorten the Li$^+$ diffusion pathways, reducing the Warburg impedance.

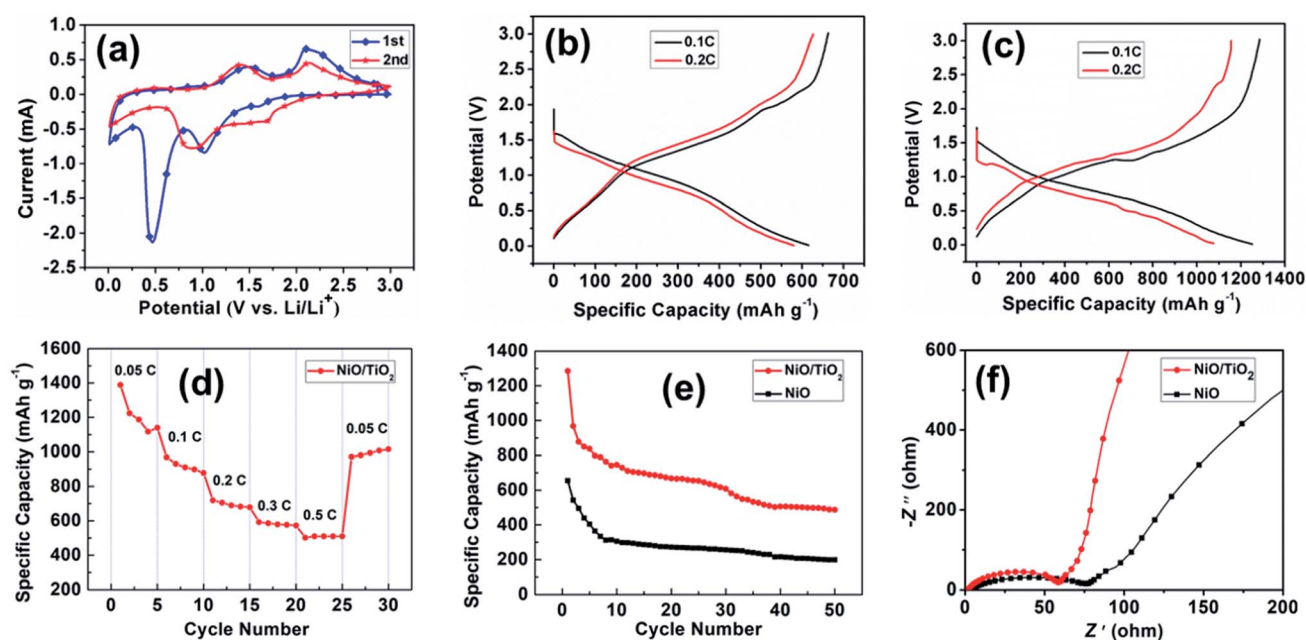Cycling performance under high charging/discharging rate was also examined to explore the potential of the NiO/TiO$_2$

Fig. 4 (a) Cyclic voltammograms of the NiO/TiO$_2$ film at a scan rate of 0.1 mV s^{-1} for the first two cycles. (b and c) Charge−discharge voltage profiles of (b) NiO and (c) NiO/TiO$_2$ electrodes at current densities of 0.1C and 0.2C. (d) Rate performance of the NiO/TiO$_2$ electrode at different current densities. (e) Cycling performance of NiO and NiO/TiO$_2$ electrodes at a current density of 0.1C. (f) Nyquist plots of NiO and NiO/TiO$_2$ electrodes.
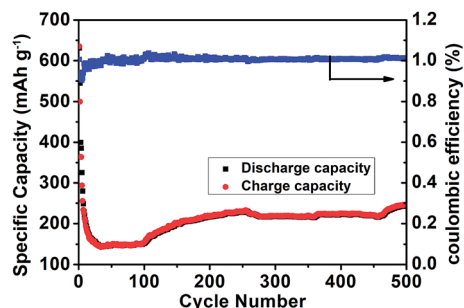
Fig. 5   Long cycling stability of the NiO/TiO$_2$ electrode at 6C.

electrode. Fig. 5 records its capacity variation under high current density of 6C (for NiO, 1C = 718 mA g^{-1}) for 500 cycles. To start with, the discharge capacity of NiO/TiO$_2$ decreases to 152.4 mA h g^{-1} in the beginning 100 cycles. Then excitingly, it increases steadily in the following cycles. Afterwards, it gradually rises to 243.9 mA h g^{-1} at the 500th cycle. Even though the capacity experiences some up and down movements, which may be related with the domination of the interfacial Li$^+$ storage mechanism, the long life under such high power is still remarkable.[32] In addition, high coulombic efficiencies (about 100% in average) are also found after the first cycle. The Fig. S2† reveal that after suffering intense cycling test, the NiO/TiO$_2$ remains original structure with uniform solid electrolyte interface (SEI) layer coating on the surface, which prevents the aggregation of the active materials. In addition, the integrity of the electrode is well preserved.

Fig. 6 outlines the proposed electron transfer and Li$^+$ diffusion mechanism during the lithiation–delithiation process. The reasons for the high electrochemical performance can be explained as follows. First, high conductive TiO$_2$ non-woven fabric film as the curren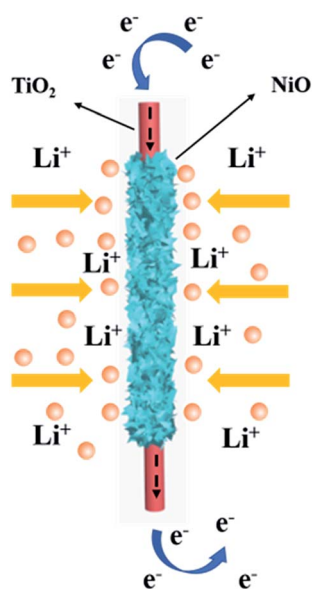t collector can enhance the electron transfer and effectively suppress the aggregation of NiO NSs, enabling the electrode material to achieve good rate capability. Second, the large interfacial areas can provide more sites for Li$^+$ storage as well as facilitate the Li$^+$ transport between the electrode and the electrolyte.[33,34]

4.   Conclusions

In conclusion, a non-woven fabric film composed of ultrathin NiO nanosheet arrays vertically grown on TiO$_2$ nanofibers has been fabricated through an electrospinning method followed by a solvothermal process. The as-fabricated NiO/TiO$_2$ electrode exhibits excellent electrochemical performance, which is attributed to the ultrathin thickness of NiO nanosheets and the direct contact with the 3D non-woven fabric TiO$_2$ film. This facile synthesis method of ultrathin NiO nanosheet arrays opens up new strategies for developing advanced electrodes for high-performance LIBs.

Conflicts of interest

There are no conflicts to declare.

Acknowledgements

References

1 M. Armand and J. M. Tarascon, *Nature*, 2008, **451**, 652–657.
2 P. G. Bruce, B. Scrosati and J. M. Tarascon, *Angew. Chem., Int. Ed.*, 2008, **47**, 2930–2946.
3 M. A. Rahman, G. Song, A. I. Bhatt, Y. C. Wong and C. Wen, *Adv. Funct. Mater.*, 2016, **26**, 647–678.
4 S. Wu, N. Du, H. Wu, C. Xiao, W. Zhao and D. Yang, *RSC Adv.*, 2016, **6**, 109649–109656.
5 Z. Wang, M. Zhang and J. Zhou, *ACS Appl. Mater. Interfaces*, 2016, **8**, 11507–11515.
6 M. V. Reddy, G. V. S. Rao and B. V. R. Chowdari, *Chem. Rev.*, 2013, **113**, 5364–5457.
7 J. Cabana, L. Monconduit, D. Larcher and M. R. Palacín, *Adv. Mater.*, 2010, **22**, E170–E192.
8 L. Zhang, J. Mu, Z. Wang, G. Li, Y. Zhang and Y. He, *J. Alloys Compd.*, 2016, **671**, 60–65.
9 J. Wu, W. Yin, W.-W. Liu, P. Guo, G. Liu, X. Liu, D. Geng, W.-M. Lau, H. Liu and L. M. Liu, *J. Mater. Chem. A*, 2016, **4**, 10940–10947.
10 Y. Feng, H. Zhang, Y. Zhang, Y. Bai and Y. Wang, *J. Mater. Chem. A*, 2016, **4**, 3267–3277.
11 P. Simon and Y. Gogotsi, *Nanosci. Tech.*, 2009, vol. 7, pp. 320–329.
12 P. Poizot, S. Laruelle, S. Grugeon, L. Dupont and J.-M. Tarascon, *Nature*, 2000, **407**, 496–499.

Fig. 6   Schematic illustration of the lithiation–delithiation process of the NiO/TiO$_2$ composite film.

13 A. K. Rai, L. T. Anh, C.-J. Park and J. Kim, *Ceram. Int.*, 2013, **39**, 6611–6618.

14 X. Shang, X. Li, H. Yue, S. Xue, Z. Liu, X. Hou and D. He, *Mater. Lett.*, 2015, **157**, 7–10.

15 H. Pang, Q. Lu, Y. Li and F. Gao, *Chem. Commun.*, 2009, 7542–7544.

16 S. A. Needham, G. X. Wang and H. K. Liu, *J. Power Sources*, 2006, **159**, 254–257.

17 V. Aravindana, P. S. Kumara, J. Sundaramurthy, W. C. Ling, S. Ramakrishn and S. Madhavia, *J. Power Sources*, 2013, **227**, 284–290.

18 D. Xie, W. Yuan, Z. Dong, Q. Su, J. Zhang and G. Du, *Electrochim. Acta*, 2013, **92**, 87–92.

19 A. K. Mondal, D. Sua, Y. Wang, S. Chen, Q. Liu and G. Wang, *J. Alloys Compd.*, 2014, **582**, 522–527.

20 J. Zhong, X. L. Wang, X. H. Xia, C. D. Gu, J. Y. Xiang, J. Zhang and J. P. Tu, *J. Alloys Compd.*, 2011, **509**, 3889–3893.

21 H. Zhang, Y. Feng, Y. Zhang, L. Fang, W. Li, Q. Liu, K. Wu and Y. Wang, *ChemSusChem*, 2014, **7**, 2000–2006.

22 J. Chen and F. Cheng, *Acc. Chem. Res.*, 2009, **42**, 713–723.

23 Y. Feng, H. Zhang, W. Li, L. Fang and Y. Wang, *J. Power Sources*, 2016, **301**, 78–86.

24 Y. Cao, Y. Dong, H. Feng, H. Chen and D. Kuang, *Electrochim. Acta*, 2016, **189**, 259–264.

25 Y. Cao, Y. Dong, H. Chen, D. Kuang and C. Su, *RSC Adv.*, 2016, **6**, 78202–78209.

26 C. A. Bonino, L. Ji, Z. Lin, O. Toprakci, X. Zhang and S. A. Khan, *ACS Appl. Mater. Interfaces*, 2011, **3**, 2534–2542.

27 B. Varghese, M. V. Reddy, Y. Zhu, S. L. Chang, T. C. Hoong, G. V. S. Rao, B. V. R. Chowdari, A. T. S. Wee, C. T. Lim and C. H. Sow, *Chem. Mater.*, 2008, **20**, 3360–3367.

28 J. Liang, H. Hu, H. Park, C. Xiao, S. Ding, U. Paik and X. Lou, *Energy Environ. Sci.*, 2015, **8**, 1707–1711.

29 X. Xu, H. Tan, K. Xi, S. Ding, D. Yu, S. Cheng, G. Yang, X. Peng, A. Fakeeh and R. V. Kumarc, *Carbon*, 2015, **84**, 491–499.

30 H. Li, H. Ma, M. Yang, B. Wang, H. Shao, L. Wang, R. Yu and D. Wang, *Mater. Res. Bull.*, 2017, **87**, 224–229.

31 S. Nilmoung, T. Sinprachim, I. Kotutha, P. Kidkhunthod, R. Yimnirun, S. Rujirawat and S. Maensiribce, *J. Alloys Compd.*, 2016, **688**, 1131–1140.

32 H. Fang, W. Zou, J. Yan, Y. L. Xing and S. C. Zhang, *ChemElectroChem*, 2018, **5**, 2458–2463.

33 W. Li, L. Zeng, Y. Wu and Y. Yu, *Sci. China Mater.*, 2016, **59**, 287–321.

34 Y. Zhou, Y. Liu, W. Zhao, F. Xie, R. Xu, B. Li, X. Zhou and H. Shen, *J. Mater. Chem. A*, 2016, **4**, 5932–5941.